Journal of Materials Chemistry C

RSC Publishing

PAPER

View Article Online
View Journal | View Issue

Cite this: J. Mater. Chem. C, 2013, 1, 4450

Containing the catalyst: diameter controlled Ge nanowire growth†

Olan Lotty,[ab] Subhajit Biswas,[ab] Tandra Ghoshal,[ab] Colm Glynn,[c] Colm O' Dwyer,[c] Nikolay Petkov,[ab] Michael A. Morris[ab] and Justin D. Holmes*[ab]

Received 6th May 2013
Accepted 11th June 2013

DOI: 10.1039/c3tc30846d

www.rsc.org/MaterialsC

Sub-20 nm diameter Ge nanowires with narrow size distributions were grown from Ag nanoparticle seeds in a supercritical fluid (SCF) growth process. The mean Ge nanowire diameter and size distribution was shown to be dependent upon Ag nanoparticle coalescence, using both spin-coating and a block copolymer (BCP) templating method for particle deposition. The introduction of a metal assisted etching (MAE) processing step in order to "sink" the Ag seeds into the growth substrate, prior to nanowire growth, was shown to dramatically decrease the mean nanowire diameter from 27.7 to 14.4 nm and to narrow the diameter distributions from 22.2 to 6.8 nm. Hence, our BCP-MAE approach is a viable route for controlling the diameters of semiconductor nanowires whilst also ensuring a narrow size distribution. The MAE step in the process was found to have no detrimental effect on the length or crystalline quality of the Ge nanowires synthesised.

Introduction

Semiconductor nanowires continue to be the subject of intense research due to their potential in scaling semiconductor devices.[1] Ge nanowires are of particular interest due to their increased mobility and Bohr radius with respect to Si.[2–4] Many studies have reported control over various aspects of nanowire growth such as doping, orientation and aspect ratio, allowing manipulation of their electrical, optical and mechanical properties.[2,5–8] Recently, supercritical fluid (SCF) growth methods have enabled the large scale production of Si and Ge nanowires in a robust, relatively inexpensive manner.[9] Various templated growth methods have been employed for growing small diameter Ge nanowires (<15 nm), including the use of anodic alumina oxide and silica membranes.[10–13] The high-diffusivity of a supercritical fluid enables rapid transport of precursors into the pores of many templates, permitting swift nucleation and growth of nanowires. Control over the pore geometry of templates has subsequently allowed the aspect ratio and optical properties of the included nanowires to be controlled with excellent precision.[14] Si nanowires, with diameters around 5 nm, have been successfully synthesized within the pores of hexagonally ordered mesoporous silicas, using a surfactant templating method.[11,15] This same technique has been used to make metallic nanowires of cobalt, copper and iron oxide[16] and has even been extended to the growth of Ge nanowires within mesoporous silica hosts.[12,13] Anodic alumina membranes (AAMs) have also been used to template the growth of Ge nanowires using both batch and injection flow-through SCF experiments.[10] In these experiments, Au colloids were used as growth catalysts inside the AAMs and the flow-through methods were found to produce better quality Ge nanowires compared to batch reactions. However, in order to release nanowires from many of these templates, harsh chemical treatments are often required which can in turn damage the nanowire surfaces. Also, the yield of nanowires from traditional templates is typically low, as the density of nanowires produced is restricted by the degree of seed inclusion within the pores of the material.

For the first time, this article reports a combined metal assisted etching (MAE) top-down approach,[17] utilizing self-assembled arrays of nanoparticles formed using block copolymer (BCP) templates,[18,19] with bottom-up SCF growth methods,[20–22] to synthesise sub-20 nm Ge nanowires with narrow diameter distributions. The novel approach described in this article of "sinking" the seed particles into the substrate by MAE prior to nanowire growth, allows total inclusion of the catalytic seeds over large areas (2 cm^2), resulting in a high yield of nanowires. Si wafers, usually used as growth substrates and collectors in SCF deposition reactions, are themselves used as templating materials. This novel combination of BCP self-assembly, top-down MAE and bottom up SCF nanowire growth

[a]Materials Chemistry and Analysis Group, Department of Chemistry, The Tyndall National Institute, University College Cork, Cork, Ireland. E-mail: j.holmes@ucc.ie; Fax: +353 (0)21 4274097; Tel: +353 (0)21 4903608

[b]Centre for Research on Adaptive Nanostructures and Nanodevices (CRANN), Trinity College Dublin, Dublin 2, Ireland

[c]Applied Nanoscience Group, Department of Chemistry, The Tyndall National Institute, University College Cork, Cork, Ireland

† Electronic supplementary information (ESI) available: PXRD pattern of nanowires grown. Comparison of all fitted diameter distributions conducted in this study. Further TEM images of nanowires grown. STEM EDX scan on Ag seeded Ge nanowire. Tabulated data on all diameter distributions measured in this work. See DOI: 10.1039/c3tc30846d

is a facile method to produce diameter controlled semiconductor nanowires, with the potential to be expanded to other materials.

Experimental

Ag nanoparticle synthesis

Ag nanoparticles were synthesized following a previously reported procedure.[23] Briefly, a solution of 300 mg of 1,2-hexadecanediol in 10 ml of 4-*tert*-butyl toluene (TBT) was heated to boiling. 100 mg of $AgNO_3$ and 1 ml of oleyamine were dissolved in 6 ml of TBT. This mixture was then injected into the hot TBT/1,2-hexadecanediol under stirring. After 5 min stirring, the system was cooled to room temperature. The Ag nanoparticles were precipitated by ethanol and washed three times with ethanol to remove free ligands, unreacted reactants, intermediates and by-products. The nanoparticles were then spin coated onto a Si substrate.

Preparation of Ag nanodots by a block copolymer inclusion technique

BCP templating was performed following a previously reported procedure.[19] Asymmetric polystyrene-*b*-poly(ethylene oxide) (PS-*b*-PEO) diblock copolymers, M_n = 42–11.5 kg mol^{-1}, M_w/M_n = 1.07; M_n = 32–11 kg mol^{-1}, M_w/M_n = 1.06 (where, M_n is the number-average molecular weight and M_w is the weight-average molecular weight) were purchased from Polymer Source and used without further purification. Si substrates were cleaned by ultrasonication in acetone and toluene for 30 min each and dried under a nitrogen stream. PS-*b*-PEO polymers were dissolved in toluene to yield a 1 wt% polymer solution at room temperature, which was subsequently aged for 12 h. A PS-*b*-PEO thin film was fabricated by spin coating the polymer solution at 3000 rpm for 30 s onto a Si substrate. The polymer films were exposed to solvent(s) placed at the bottom of a closed vessel at a temperature of 50 °C to induce necessary chain mobility and allow microphase separation to occur. The PS-PEO (32-11) film was exposed to toluene for 2 h and toluene–water (50 : 50, v/v) mixed vapour was used for the PS-PEO (42-11.5) films under static vacuum for 1 h. Partial etching and domain modification of PEO was carried out by ultrasonication of the films in anhydrous alcohol for different time periods. After 15 min the films were removed from the alcohol and dried immediately. For the fabrication of Ag nanodots, 0.5 wt% solutions of $AgNO_3$ were dissolved in ethanol and spin-coated onto the nanoporous films. UV/ozone treatment was used to remove the remaining polymer.

Metal assisted etching (MAE)

After deposition (non-templated Ag nanoparticles or BCP patterned Ag nanodots), the catalytic particles were etched in a solution consisting of H_2O, 49% HF and 30% H_2O_2 in the ratio of 46 : 3 : 1 at 50 °C for 2 min.

Supercritical fluid growth of Ge nanowires

Diphenylgermane (DPG) was used as the Ge precursor for nanowire growth. The metal-seeded growth of Ge nanowires was performed in supercritical toluene using a method previously reported.[22] In a typical experiment a 5 ml stainless steel reaction cell (HIP, USA) was loaded with 2 ml of anhydrous toluene and sealed inside a nitrogen filled glovebox. The reaction cell was then transferred to a tube furnace where it was heated to the desired reaction temperature and allowed to equilibrate for a period of 2 h. A DPG precursor solution (10 mM) was prepared in anhydrous toluene (20 ml) in an N_2 glovebox and loaded into a 20 ml stainless steel precursor reservoir (HIP, USA). This reservoir was then removed from the glovebox and connected to the reaction cell by 1/16″ stainless steel tubing and valves. A back pressure of 17.2 MPa was applied to the precursor reservoir; this solution was injected at the chosen synthesis temperature using a CO_2 pump (ISCO systems). A typical injection rate used was 0.025 ml min^{-1} for varying times.

Characterisation

Energy dispersive X-ray (EDX) analysis was performed using an Oxford Instruments INCA system fitted to a scanning electron microscope. Powder X-ray diffraction (PXRD) analysis was performed on a Phillips Xpert PW3719 diffractometer using Cu KR radiation (40 kV and 35 mA) over the range $10 < 2\theta < 70$. Atomic Force Microscope (SPM, Park systems, XE-100) was operated in AC (tapping) mode under ambient conditions using silicon microcantilever probe tips with a force constant of 60 000 N m^{-1} and a scanning force of 0.11 nN. Topographic and phase images were recorded simultaneously. SEM imaging was carried out on a FEI Helios Nanolab™ dual-beam SEM/FIB suite operating at 5–10 kV. Transmission electron microscopy (TEM) images were collected using a JEOL 2100 HRTEM instrument operating at an acceleration voltage of 200 kV. In all cases, samples were prepared for analysis by sonicating the material in isopropyl alcohol (IPA) before TEM sample preparation. Statistical analysis and fitting of the measured core diameter distributions of the nanowires was performed using Origin Pro v.8.5.1 and over 120 measurements were used for every nanowire diameter distribution. Raman Spectroscopy was collected with a Renishaw InVia Raman spectrometer using a 514 nm 30 mW Argon Ion laser. Spectra were collected using a RenCam CCD camera. The beam was focused onto the samples using a 50× objective lens.

Results and discussion

The movement and combination of metal seed nanoparticles on a surface can result in particle aggregation. These aggregated metal particles result in the evolution of nanowires many times larger than the size of the original seeds.[1,24] There are two limiting cases of dimensional changes reported for nanoparticles on a surface. The first, coalescence, is whereby particles adhere poorly to a surface, permitting them to diffuse across a substrate and coalesce. The second, Ostwald ripening, is when a nanoparticle adheres strongly to a surface, making atomic transfer between nanoparticles more favourable than coalescence.[25] Both of these processes generally follow the von

Smoluchowski kinetic rate equation, $d \propto t^{-\alpha}$, where d is the nanoparticle diameter, t is time and α is a constant relating to interfacial adhesion. The processes differ in the magnitude of α, which decreases with increasing particle–substrate interfacial adhesion.[25,26] Au nanoparticles have been used to catalyse the SCF growth of Ge nanowires in many studies, *via* a supercritical-fluid–liquid–solid (SFLS) growth mechanism.[27–29] The use of Au as a catalytic material for Ge nanowire growth is common due to the relatively low temperatures at which the Au–Ge eutectic is formed, allowing the rapid nucleation and growth of nanowires. However, the Au–Ge liquid eutectic has also been shown to be detrimental to the integrity of the nanowires, *e.g.* large diameter distribution and unintentional doping, due to the high mobility of Au both on the growth substrate and also within the nanowires.[24,30] The issue of Au nanoparticle coalescence prior to nanowire growth has also been studied by Gou *et al.*,[31] who suggest that a buffer layer forms on the substrate surface, thereby enabling coalescence events which are affected by both the metal vapour pressure and the density of nanoparticles on the surface. Solid phase seeding of Si and Ge nanowires from SCFs, in an attempt to prevent inadvertent doping of the nanowires during the growth process and also to narrow their diameter distributions, has also been reported.[22,32] In particular, solid phase seeding of Ge nanowires with Ni, Cu, Ti and Ag nanoparticles has recently being reported.[20,22,32–37] However, some of these solid phase catalysts form germanides, resulting in a dramatic expansion of the catalyst seed.[20] Of these potential solid seeds, only Al and Ag do not form germanides and of these, only Ag has anisotropic etch behavior in Si.[20,38] For these reasons, Ag nanoparticles were chosen as the catalyst for Ge nanowire growth in this study. The Ge nanowire growth in this study proceeds *via* a supercritical fluid–solid–solid (SFSS) growth mechanism. The liquid eutectic, which is characteristic of the SFLS growth mechanism, is not formed in a SFSS procedure. Instead, the Ge atoms diffuse through or around the solid lattice of the metal seed and crystallise at the highest energy facet available.[22] As no liquid eutectic is necessary for growth to proceed by this mechanism, nanowires can be produced far below the eutectic temperature of the alloy; often termed sub-eutectic growth. Even solid phase catalysts can undergo surface diffusion on Si surfaces by coalescence or Ostwald ripening before and during growth. As the bulk melting temperature of Ag is 1235 K and the temperature of our growth system is ~700 K, particle diffusion along a Si surface may seem unlikely. However, an examination of both the Tammann temperature and the melting point depression of nanoparticles show that particle movement is highly probable. The sintering of metal is strongly temperature dependant and closely related to the Tammann temperature, where the Tammann temperature is defined as approximately half of the melting temperature.[39] This is the temperature at which the bulk atoms of a particle will exhibit mobility.[40] Also, as is widely reported, nanoparticles undergo a melting point depression due to an increased surface : bulk atom ratio. For Ag, the bulk melting point of 1235 K may be applicable only to nanoparticles with diameters >100 nm; Ag nanoparticles with diameters below 100 nm are subject to a depressed melting point, as shown in eqn (1) below. Eqn (1) describes a general relationship for the size and shape dependant melting temperature of crystals:[41]

$$T_m = T_{mb}\left(1 - 6\alpha\frac{r}{D}\right) \quad (1)$$

where T_m is the depressed melting temperature of a Ag nanoparticle of diameter D (in nm), T_{mb} is the bulk melting temperature of Ag (1235 K), α is a shape constant ($\alpha = 1$ for spherical particles) and r is the atomic radius of Ag (0.144 nm).

The growth temperature used to synthesise Ge nanowires in this study was 703 K, which lies well above the Tammann temperature for nanoparticles of that size (Fig. 1). Fig. 1 shows a theoretical graph of the melting point of Ag nanoparticles (T_m) as a function of nanoparticle diameter (D), with a superimposed graph of the Tammann temperature for Ag nanoparticles as a function diameter.

Fig. 2 shows a TEM image of some Ag nanoparticles used as growth seeds for Ge nanowires, along with their diameter distribution. These nanoparticles were spin coated onto Si substrates from a toluene suspension and the solvent was allowed to evaporate overnight to ensure sufficient particle–surface adhesion. Fig. 2(c) is an SEM image illustrating the network of Ge nanowires produced from the Ag seeds. Most of the Ge nanowires synthesised had a length greater than 5 μm for a reaction time of 5 h and a primary growth direction of ⟨112⟩ for twinned nanowires and ⟨111⟩ for untwined nanowires, consistent with previous reports.[42] As shown in Fig. 2, there is a large discrepancy between the mean diameter of the Ge nanowires grown (32.3 ± 15.3 nm) and the Ag nanoparticles used to seed the growth (9.3 ± 2.5 nm), due to the aggregation of seed particles before and perhaps during the nanowire growth process.

In an attempt to prevent the coalescence of nanoparticles on the surface of Si substrates, metal assisted etching (MAE) was employed to "sink" or etch the Ag nanoparticles into the Si surface prior to Ge nanowire growth. As before, the Ag nanoparticles were deposited onto a Si substrate by spin coating. The deposited Ag nanoparticles were then etched into the substrate

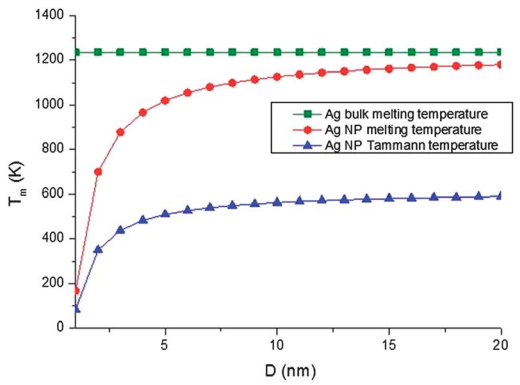

Fig. 1 Graph showing melting point depression of Ag nanoparticles as a function of nanoparticle diameter (red) and the Tammann temperature as a function of nanoparticle diameter (blue). Also included is the bulk melting temperature of Ag (green).

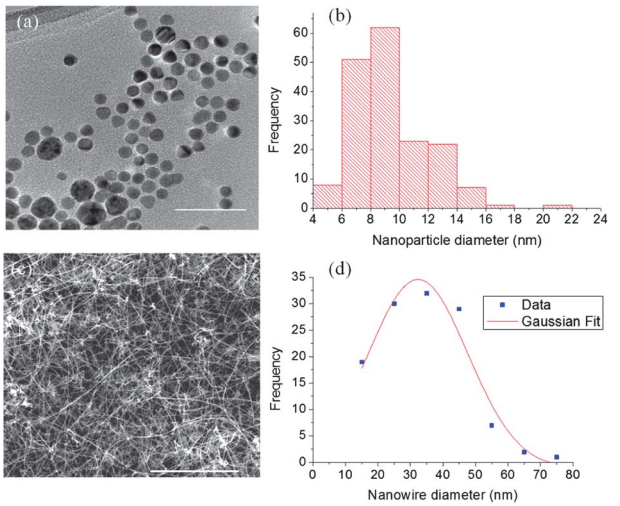

Fig. 2 (a) TEM image of the Ag nanoparticles used to seed the growth of Ge nanowires (scale bar = 50 nm), (b) nanoparticle diameter distribution (170 nanoparticles) of the same Ag nanoparticles showing a mean diameter of 9.3 ± 2.5 nm, (c) SEM image of Ge nanowires grown from the Ag nanoparticles shown in (a) (scale bar = 5 μm) and (d) diameter distribution of the Ge nanowires showing a mean diameter of 32.3 ± 15.3 nm (FWHM = 36.1 nm).

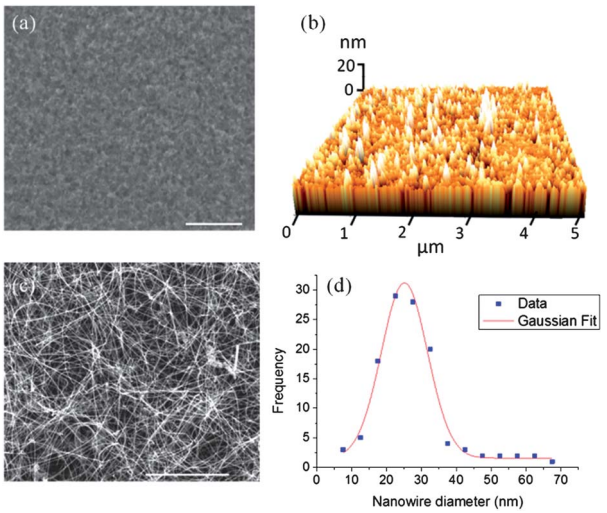

Fig. 3 (a) SEM image of Si substrate after undergoing MAE (scale bar = 1 μm) and (b) AFM topography study illustrating the roughness of the same Si surface after undergoing MAE, (c) SEM image of Ge nanowires grown from the sunken nanoparticles (scale bar = 2 μm) and (d) nanowire diameter distribution the Ge nanowires grown from the Ag nanoparticles etched into the Si, showing the mean diameter of 25.1 ± 6.6 nm.

using an etchant solution containing both HF and the oxidant H_2O_2. The etching mechanism of Si in a solution of HF and H_2O_2 is based upon hole injection.[43] The electrochemical potential of H_2O_2 is much more positive than the valence band of Si and more positive than the other oxidants usually used in the stain etching of Si ($KMnO_4$, $KBrO_3$, $K_2Cr_2O_7$, *etc.*).[43] Holes are generated at the metal particle, which can be viewed as the cathode in terms of an electrochemical reaction. Holes are generated by the reduction of H_2O_2, shown in eqn (2):

$$H_2O_2 + 2H^+ \rightarrow 2H_2O + 2h^+ \quad (2)$$

These holes then contribute to the oxidation and subsequent dissolution of the underlying Si substrate in the HF solution as shown in eqn (3) and (4):

$$Si + 4h^+ + 4HF \rightarrow SiF_4 + 4H^+ \quad (3)$$

$$SiF_4 + 2HF \rightarrow H_2SiF_6 \quad (4)$$

Fig. 3(a) shows an SEM image of the surface of a Si substrate after etching along with an AFM surface profile of the same sample (Fig. 3(b)). AFM topography studies and cross sectional SEM imaging show that the mean etch depth was approximately 175 nm but was as deep as 300 nm in parts of the substrate. The sinking of the Ag nanoparticles into the substrate would considerably change the particle–substrate interfacial energy from the smooth polished Si wafer before etching, creating both a physical and energetic barrier to surface diffusion of the Ag nanoparticles before and during growth of Ge nanowires. Although there is no evidence to suggest that Ag nanoparticles used in MAE are chemically bound to the etched Si substrate, the migration of holes though the metal particle could possibly increase the adhesion between the particle and substrate.[43] The exact same growth conditions were employed for synthesising Ge nanowires from the sunken MAE Ag nanoparticles as those previously spin-coated onto a Si substrate. From SEM and TEM studies, no apparent changes in the lengths or observed primary growth directions of the Ge nanowires were detected compared to those grown from Ag nanoparticles that were not etched into the substrate. Both seeds produced Ge nanowires with high aspect ratios, however the nanowires grown from the nanoparticles etched into the substrate had a much smaller mean diameter of 25.1 ± 6.6 nm with a narrow diameter distribution (FWHM = 15.6 nm).

Although a shift towards smaller diameter Ge nanowires and some narrowing of the diameter distribution was seen upon etching the metal seed catalysts into the Si substrate before growth, the mean diameter of the nanowires still lies reasonably far from the mean diameter of the initial seed nanoparticles used (9.3 ± 2.5 nm, Fig. 2). The discrepancy between the diameter of the Ge nanowires and the diameters of the Ag nanoparticles used to seed their growth can be explained by the nature of the Ag particles themselves and how they are deposited onto the substrate. The Ag particles are oleylamine stabilized in order to prevent them from agglomerating. However the interparticle separation that this type of stabilisation offers on the substrate is of the same order of magnitude of the capping ligand ~2 nm.[44] This interparticle separation can be increased by varying the spin coating parameters, but this often results in areas of dense nanoparticle coverage interspaced by vast areas of scarce nanoparticle coverage. Ag nanoparticles that are not well separated can "etch as one" under MAE conditions and subsequently coalesce to seed the growth of larger diameter Ge nanowires. Also, the aqueous, acidic nature of the etching reaction can destabilize and mobilize nanoparticles on the surface of a Si substrate, bringing them closer into contact than

before. As some may etch as coalesced aggregates and others may not, the mean diameter and diameter distribution of the Ge nanowires produced is further apart than anticipated from the mean diameter and diameter distribution of the etched Ag nanoparticles used to seed their growth. Block copolymer (BCP) self-assembly offers a cheap, non-lithographic method of pre-patterning metallic nanoparticles on a surface and can be used to increase the interparticle separation and hence reduce the coalescence of nanoparticles. Recently, we demonstrated a facile generic method for fabricating high density arrays of hexagonally ordered inorganic nanodots on Si substrates over large areas using polystyrene-*b*-poly(ethylene oxide) (PS-*b*-PEO) BCP thin films as a structural template.[18,19] This method is particularly useful as the feature sizes of the dots can be tuned by changing the concentration and the molecular weight of the BCP. The Ag nanodots that were formed in this process (13.7 ± 1.5 nm, Fig. 4) were slightly larger than the nanoparticles used earlier (9.3 ± 2.5 nm). Nonetheless, the separation of Ag seed particles that this templating method offers over a large area (2 cm^2), is far superior to those achievable by spin coating the nanoparticles. Fig. 4 is a schematic of the BCP templating method used, along with an SEM image of the resulting nanodot structure.

Ge nanowires were grown from the BCP patterned nanodots on the surface and also from BCP patterned nanodots that had undergone MAE. As before, no differences in the length or nominal growth direction were observed between the Ge nanowires grown in both cases, or from the Ge nanowires grown from the non-templated Ag nanoparticles. However a dramatic shift in the mean diameter and the diameter distribution of Ge nanowires was observed for the Ge nanowires grown from the templated Ag nanodots. The Ge nanowires grown from Ag nanodots that had undergone both BCP patterning and MAE had a mean diameter of 14.4 ± 2.9 nm (FWHM = 6.8 nm), in close agreement with the diameter of the BCP patterned Ag nanodots used as the growth catalyst (13.7 ± 1.5 nm, FWHM = 3.5 nm). The nanowires grown from the BCP nanodots on the surface showed a mean diameter of 27.7 ± 9.4 nm (FWHM = 22.2 nm) indicating that the interparticle separation offered by BCP patterning alone is not enough to prevent particle coalescence or aggregation at the reaction temperature of 703 K. These results are summarised in Fig. 5 and are also tabulated in ESI, Table S1.†

Analysis of the (111) and (220) XRD peaks for both the Ge nanowires grown from the BCP patterned Ag nanodots and from the BCP nanodots after MAE showed no shift in peak position with respect to each sample. A PXRD pattern for the nanowires produced can be found in ESI, Fig. S1.† A technique first reported by Warren[45] that was used to examine the effects of annealing on the defect density in a crystallite was adapted to our system, as shown in eqn (5):

$$\Delta(2\theta_{220} - 2\theta_{111}) \propto \alpha \quad (5)$$

where α is the deformation fault density and $\Delta(2\theta_{220} - 2\theta_{111})$ is the difference in peak separation compared to that expected for no faulting (in our case, bulk Ge).[46] As the value of $\Delta(2\theta_{220} - 2\theta_{111})$ is directly proportional to the deformation fault density, this value of $\Delta(2\theta_{220} - 2\theta_{111})$ can be compared in both samples to see if the deformation fault density has changed. For both BCP patterned nanowire samples, this value was shown to be equal at $\Delta(2\theta_{220} - 2\theta_{111}) = 0.09$, hence the deformation fault density did not increase upon the introduction of the MAE step. A comparison of the twin fault density for both the Ge nanowires grown from the BCP patterned Ag nanodots and from the BCP nanodots after MAE was performed using a method recently reported by Ingham *et al.*[46] The Scherrer equation was used to calculate the coherence length, D_{eff}, for both the (111) and (220) reflections and these values were then used to solve for a value of $(1.5\alpha + \beta)$, following the expression shown in eqn (6):

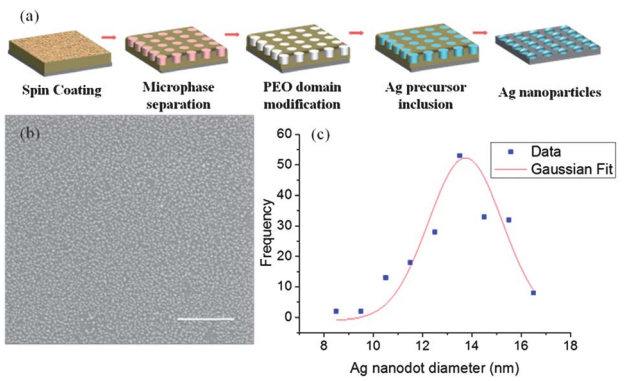

Fig. 4 (a) Schematic showing the BCP self-assembly process used to congregate Ag nanoparticles on the surface of a Si substrate, (b) SEM image of Ag nanodots on the surface of a Si substrate (scale bar = 500 nm) and (c) diameter distribution of the Ag nanodots showing the mean diameter to be 13.7 ± 1.5 nm.

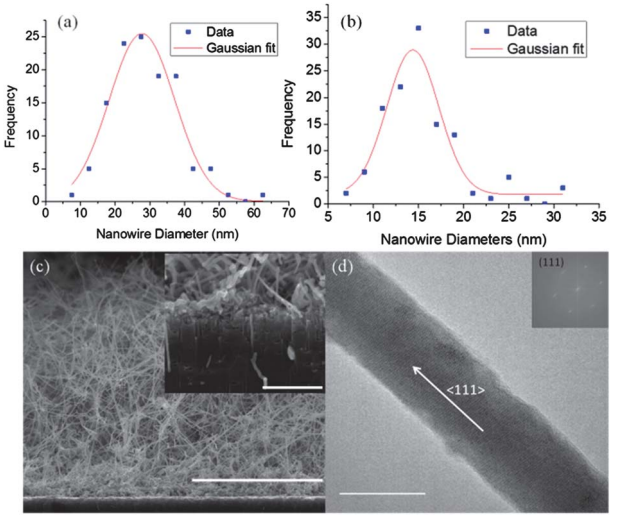

Fig. 5 (a) Diameter distributions of Ge nanowires grown from BCP patterned Ag nanodots and (b) Ge nanowires grown from BCP nanodots after MAE. (c) SEM cross sectional image of Ge nanowires grown from BCP patterned and MAE Ag nanodots (scale bar = 3 μm), with higher magnification inset showing Ge nanowires protruding from etched holes (scale bar = 500 nm). (d) TEM image of a resulting Ge nanowire grown along ⟨111⟩ growth direction with FFT inset showing the highly crystalline nature of the sample (scale bar = 20 nm). More TEM images can be found in ESI, Fig. S3.†

$$\frac{1}{D_{\text{eff}}^2} = \frac{1}{D^2} + \frac{(1.5\alpha + \beta)^2}{a^2} C_{hkl}^2 \quad (6)$$

where β is the twin fault density, a is the cubic lattice parameter, D is the crystallite size and C_{hkl} is a numeric factor, having values of 0.43 for the (111) reflection and 0.71 for the (220) reflection.[47] From these calculations it was found that the Ge nanowires grown from the etched nanodots had a much lower twinning fault density with a value of $(1.5\alpha + \beta) = 0.0079$, compared to the Ge nanowires grown from the unetched nanodots which yielded a value of $(1.5\alpha + \beta) = 0.0182$. A twin plane can occur through the coalescence of seed particles which can in turn be translated into the growing nanowire (ESI, Fig. S3(c)†).[20,37] The etched nanodots partake in considerably less coalescence events and so the likelihood of twinning faults propagating from the seed particles to the nanowires is reduced. TEM evidence also supports this, with almost 50% of the Ge nanowires grown from the nanodots on the surface displaying axial twinning faults (these twinned nanowires all had a growth direction of ⟨112⟩) compared to just 34% for the Ge nanowires grown from the nanodots etched into the surface.

Ge nanowire samples from both the BCP patterned etched and unetched nanodots were examined by Raman spectroscopy. As shown in Fig. 5, the nominal diameter of the nanowires from the etched nanodots were considerably smaller (centered at 14.4 nm) than those from the unetched nanodots (centered at 27.7 nm). This difference was also reflected in the full width half maximum (FWHM) of the first order Raman peaks of the nanowires, compared in Fig. 6 below. No significant peak shift was seen between the two samples (both peaks appear at 300 cm^{-1}), but the smaller diameter nanowires (14.4 nm) had a broader, more asymmetric peak with a FWHM of 6.2 cm^{-1} compared to the larger nanowires (27.7 nm) with a FWHM of only 5.6 cm^{-1}. This difference in shape and width of the Raman peak is typically attributed to the increased quantum confinement of optical phonons in the smaller Ge nanowires due to the diameter size effects.[48] However, quantitative determination of size and diameter effects in bundles of nanowires is difficult due to the lack of a peak shift between the nanowire samples and bulk Ge that would be expected for a dominant contribution from confinement effects. It can be assumed that twin planes observed within the nanowires also contribute to the broadening and asymmetry seen in the scattering spectrum.

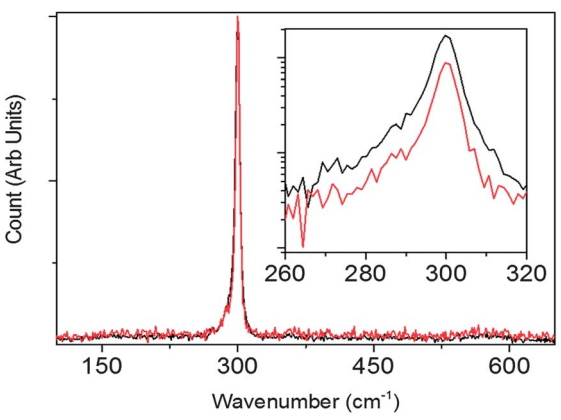

Fig. 6 Raman spectra of Ge nanowires grown from BCP patterned nanodots (red trace) and from BCP patterned and MAE nanodots (black trace).

Conclusions

In conclusion, sub-20 nm Ge nanowires have been grown from Ag nanoparticles. The problem of particle coalescence, leading to the growth of larger diameter nanowires, has been minimised by introducing a MAE step after particle deposition but before nanowire growth. This MAE step has been shown to lower the mean diameter and narrow the diameter distribution of the nanowires grown. A pre-patterning BCP process, prior to the MAE step, has been shown to make even greater improvements to the mean diameter and diameter distribution and furthermore without any detrimental effect on the length or increase in the defect density of the nanowires produced. This integrated nanowire growth approach has wide implications for the mass production of bottom up semiconducting nanowires with uniform diameters and may be transferred to other growth systems whereby the catalytic seed can be etched into the Si substrate. Using e-beam lithography in order to place the catalyst more precisely, in conjunction with MAE, prior to nanowire growth may also offer a route to interesting hetero-materials or to nanowire interconnects in a 3D chip assembly.

Acknowledgements

We acknowledge financial support from the EU 7th Framework Programme under the SiNAPS project (Grant: 257856) and Science Foundation Ireland (Grant: 09/IN.1/I2602). This research was also enabled by the Higher Education Authority Program for Research in Third Level Institutions (2007–2011) *via* the INSPIRE programme.

Notes and references

1 M. Koto, A. F. Marshall, I. A. Goldthorpe and P. C. McIntyre, *Small*, 2010, **6**, 1032–1037.
2 X. Y. Wu, J. S. Kulkarni, G. Collins, N. Petkov, D. Almecija, J. J. Boland, D. Erts and J. D. Holmes, *Chem. Mater.*, 2008, **20**, 5954–5967.
3 T. Hanrath and B. A. Korgel, *J. Am. Chem. Soc.*, 2004, **126**, 15466–15472.
4 A. G. Cullis, L. T. Canham and P. D. J. Calcott, *J. Appl. Phys.*, 1997, **82**, 909–965.
5 M. I. van der Meulen, N. Petkov, M. A. Morris, O. Kazakova, X. Han, K. L. Wang, A. P. Jacob and J. D. Holmes, *Nano Lett.*, 2008, **9**, 50–56.
6 I. R. Musin and M. A. Filler, *Nano Lett.*, 2012, **12**, 3363–3368.
7 S. A. Dayeh and S. T. Picraux, *Nano Lett.*, 2010, **10**, 4032–4039.
8 V. C. Holmberg, T. D. Bogart, A. M. Chockla, C. M. Hessel and B. A. Korgel, *J. Phys. Chem. C*, 2012, **116**, 22486–22491.
9 T. Zhai and J. Yao, *One-dimensional nanostructures: Principles and applications*, Wiley, 2012.

10 N. Petkov, P. Birjukovs, R. Phelan, M. A. Morris, D. Erts and J. D. Holmes, *Chem. Mater.*, 2008, **20**, 1902–1908.
11 N. R. B. Coleman, N. O'Sullivan, K. M. Ryan, T. A. Crowley, M. A. Morris, T. R. Spalding, D. C. Steytler and J. D. Holmes, *J. Am. Chem. Soc.*, 2001, **123**, 7010–7016.
12 N. R. B. Coleman, K. M. Ryan, T. R. Spalding, J. D. Holmes and M. A. Morris, *Chem. Phys. Lett.*, 2001, **343**, 1–6.
13 K. Ziegler, K. M. Ryan, R. Rice, T. Crowley, D. Erts, H. Olin, J. Patterson, T. R. Spalding, J. D. Holmes and M. A. Morris, *Faraday Discuss.*, 2004, **125**, 311–326.
14 K. M. Ryan, D. Erts, H. Olin, M. A. Morris and J. D. Holmes, *J. Am. Chem. Soc.*, 2003, **125**, 6284–6288.
15 D. M. Lyons, K. M. Ryan, M. A. Morris and J. D. Holmes, *Nano Lett.*, 2002, **2**, 811–816.
16 T. A. Crowley, K. J. Ziegler, D. M. Lyons, D. Erts, H. Olin, M. A. Morris and J. D. Holmes, *Chem. Mater.*, 2003, **15**, 3518–3522.
17 X. Li and P. W. Bohn, *Appl. Phys. Lett.*, 2000, **77**, 2572–2574.
18 T. Ghoshal, T. Maity, J. F. Godsell, S. Roy and M. A. Morris, *Adv. Mater.*, 2012, **24**, 2390–2397.
19 T. Ghoshal, M. T. Shaw, C. T. Bolger, J. D. Holmes and M. A. Morris, *J. Mater. Chem.*, 2012, **22**, 12083–12089.
20 S. Barth, J. J. Boland and J. D. Holmes, *Nano Lett.*, 2011, **11**, 1550–1555.
21 S. Barth, F. Hernandez-Ramirez, J. D. Holmes and A. Romano-Rodriguez, *Prog. Mater. Sci.*, 2010, **55**, 563–627.
22 S. Barth, M. M. Koleśnik, K. Donegan, V. Krstić and J. D. Holmes, *Chem. Mater.*, 2011, **23**, 3335–3340.
23 Q. B. Zhang, J. P. Xie, J. H. Yang and J. Y. Lee, *ACS Nano*, 2009, **3**, 139–148.
24 J. B. Hannon, S. Kodambaka, F. M. Ross and R. M. Tromp, *Nature*, 2006, **440**, 69–71.
25 M. Jose-Yacaman, C. Gutierrez-Wing, M. Miki, D. Q. Yang, K. N. Piyakis and E. Sacher, *J. Phys. Chem. B*, 2005, **109**, 9703–9711.
26 D. Q. Yang and E. Sacher, *Appl. Surf. Sci.*, 2003, **207**, 1–5.
27 G. Collins, M. Koleśnik, V. Krstić and J. D. Holmes, *Chem. Mater.*, 2010, **22**, 5235–5243.
28 T. Hanrath and B. A. Korgel, *J. Am. Chem. Soc.*, 2002, **124**, 1424–1429.
29 B. Yoo, A. Dodabalapur, D. C. Lee, T. Hanrath and B. A. Korgel, *Appl. Phys. Lett.*, 2007, **90**, 072166-1.
30 A. M. Chockla and B. A. Korgel, *J. Mater. Chem.*, 2009, **19**, 996–1001.
31 D. L. Guo, X. Huang, G. Z. Xing, Z. Zhang, G. P. Li, M. He, H. Zhang, H. Chen and T. Wu, *Phys. Rev. B: Condens. Matter Mater. Phys.*, 2011, **83**, 045403.
32 H.-Y. Tuan, D. C. Lee, T. Hanrath and B. A. Korgel, *Nano Lett.*, 2005, **5**, 681–684.
33 H.-Y. Tuan, D. C. Lee, T. Hanrath and B. A. Korgel, *Chem. Mater.*, 2005, **17**, 5705–5711.
34 H.-Y. Tuan, A. Ghezelbash and B. A. Korgel, *Chem. Mater.*, 2008, **20**, 2306–2313.
35 C. A. Barrett, R. D. Gunning, T. Hantschel, K. Arstila, C. O'Sullivan, H. Geaney and K. M. Ryan, *J. Mater. Chem.*, 2010, **20**, 135–144.
36 H. Geaney, C. Dickinson, C. A. Barrett and K. M. Ryan, *Chem. Mater.*, 2011, **23**, 4838–4843.
37 S. Biswas, A. Singha, M. A. Morris and J. D. Holmes, *Nano Lett.*, 2012, **12**, 5654–5663.
38 O. Lotty, N. Petkov, Y. M. Georgiev and J. D. Holmes, *Jpn. J. Appl. Phys.*, 2012, **51**, 11PE03.
39 J. M. Sun, D. Ma, H. Zhang, X. M. Liu, X. W. Han, X. H. Bao, G. Weinberg, N. Pfander and D. S. Su, *J. Am. Chem. Soc.*, 2006, **128**, 15756–15764.
40 J. A. Moulijn, A. E. van Diepen and F. Kapteijn, *Appl. Catal., A*, 2001, **212**, 3–16.
41 W. H. Qi and M. P. Wang, *Mater. Chem. Phys.*, 2004, **88**, 280–284.
42 F. M. Davidson, D. C. Lee, D. D. Fanfair and B. A. Korgel, *J. Phys. Chem. C*, 2007, **111**, 2929–2935.
43 Z. P. Huang, N. Geyer, P. Werner, J. de Boor and U. Gosele, *Adv. Mater.*, 2011, **23**, 285–308.
44 Z. Wang, X.-D. Wen, R. Hoffmann, J. S. Son, R. Li, C.-C. Fang, D.-M. Smilgies and T. Hyeon, *Proc. Natl. Acad. Sci. U. S. A.*, 2010, **107**, 17119–17124.
45 B. E. Warren, in *X-ray Diffraction,* Dover Publications Inc., New York, 1969.
46 B. Ingham, T. H. Lim, C. J. Dotzler, A. Henning, M. F. Toney and R. D. Tilley, *Chem. Mater.*, 2011, **23**, 3312–3317.
47 C. N. J. Wagner, *Acta Metall.*, 1957, **5**, 427–434.
48 Y. F. Zhang, Y. H. Tang, N. Wang, C. S. Lee, I. Bello and S. T. Lee, *Phys. Rev. B: Condens. Matter Mater. Phys.*, 2000, **61**, 4518–4521.